Physics-Informed Domain Generalization for Bearing Prognostics Under Unseen Operating Conditions

Seyed Ali Hosseinli[1, 2] and Konstantinos Gryllias[1, 2]

[1] *Department of Mechanical Engineering, KU Leuven*
[2] *Flanders Make @ KU Leuven*
Celestijnenlaan 300, BOX 2420, 3001 Leuven, Belgium
ali.hosseinli@kuleuven.be

ABSTRACT

Modern condition-based maintenance of rotating machinery increasingly relies on data-driven prognostic models to estimate bearing health and remaining useful life (RUL). While machine-learning approaches have demonstrated strong performance under known operating conditions, their reliability often degrades under unseen loads, speeds, and degradation regimes, limiting their industrial applicability. This work addresses bearing prognostics under unseen operating conditions through a physics-informed real-to-real transfer learning framework. To improve physical consistency and long-term prognostic stability, the proposed approach incorporates constraints inspired by fatigue crack growth theory into the learning process. In particular, monotonic degradation behavior consistent with Paris-law-type dynamics is enforced by learning bias, promoting physically plausible degradation evolution and RUL estimation. Building on this physics-guided foundation, the framework further addresses domain shifts through domain generalization and feature disentanglement. The method accounts for both marginal and conditional domain shifts across multiple source domains representing different operating conditions and degradation trajectories. By disentangling domain-invariant degradation features from domain-specific operational characteristics, the model enables zero-shot generalization to previously unseen target conditions without requiring target-domain data. The proposed method is validated using experimental bearing run-to-failure datasets and demonstrates robust prognostic performance under unseen operating conditions while maintaining physically consistent degradation behavior. The results highlight the potential of combining physics-informed learning with domain generalization for reliable industrial bearing prognostics.

1. INTRODUCTION

Rolling element bearings are critical components in rotating machinery across transportation, energy, manufacturing, and aerospace industries. Their degradation can lead to catastrophic failures, unplanned downtime, and economic losses. In high-value assets such as wind turbines, railway traction systems, and aeroengines, bearing failures not only incur repair costs but may also compromise safety and operational continuity. Consequently, accurate estimation of bearing remaining useful life (RUL) has become a central objective of modern condition-based maintenance and prognostics frameworks.

The dominant life-limiting mechanism in bearings is rolling contact fatigue (RCF), in which cyclic Hertzian contact stresses drive the accumulation of microstructural damage until cracks initiate and propagate, ultimately causing spalling or pitting (Kunzelmann et al., 2023; Rycerz et al., 2017). Beyond a threshold crack length, surface-initiated crack growth has been shown to approximately follow Paris-law-type behavior in the stable propagation regime (Kunzelmann et al., 2023). The underlying fracture-mechanics formulation is summarized in Section 2.

This fatigue-mechanics foundation has motivated a broad family of physics-based prognostic methods. Early approaches embedded linear elastic fracture mechanics (LEFM) crack-growth models such as Paris' law within recursive Bayesian and particle-filtering frameworks, formulating fatigue crack propagation as a stochastic state-space model and sequentially updating both crack state and model parameters from measurements (Chen et al., 2018; Hosseinpour et al., 2020; Liu et al., 2017; L. Wang et al., 2023). Related work has also combined Paris-law physics with digital-twin schemes that jointly estimate defect size and vibration response (Shi et al., 2026). Despite their effectiveness, these methods generally assume an explicit stochastic state-space representation in which crack length evolves according to a fracture-mechanics growth model

and is linked to observations through a predefined measurement equation, thereby requiring either direct crack measurements or engineered degradation indicators with a known functional relationship to crack length.

Physics-informed neural networks (PINNs) offer a different paradigm. Rather than imposing Paris' law as a rigid state-transition equation, they embed fatigue dynamics as a soft constraint within a representation-learning framework, allowing latent degradation trajectories to be learned directly from raw sensor data while remaining consistent with crack-growth behavior; in this setting, physics acts as a regularizing prior rather than a fixed parametric assumption. Recent studies introduce Paris-law regularization within neural RUL predictors (Dhibi et al., 2026), shape the health indicator using fatigue-damage mechanisms (Ta et al., 2026), or model fatigue accumulation through physics-based cumulative-damage layers combined with data-driven components (Yucesan & Viana, 2023). These works demonstrate that fatigue-inspired constraints improve interpretability and stability, but they typically target prediction accuracy within known domains rather than systematic generalization to unseen operating regimes.

This generalization gap is the central practical obstacle to industrial deployment. Deep models achieve strong accuracy under controlled, stationary conditions, but their performance degrades under unseen loads, speeds, lubrication regimes, or material variations (Han et al., 2026). In realistic environments, these factors induce both marginal distribution shifts (changes in input statistics) and conditional shifts (changes in degradation trajectories for similar signals). Conventional domain adaptation mitigates marginal shifts by extracting domain-invariant features, but it generally requires unlabeled target-domain data (Da Costa et al., 2020; Dong et al., 2023; Hosseinli et al., 2023), which is unavailable when the target regime cannot be accessed or when collecting data for every operating condition is infeasible (Han et al., 2026). Moreover, an exclusive focus on invariant features can discard domain-specific information that is useful within particular conditions (Bui et al., 2021).

Domain generalization (DG) addresses these limitations by learning from multiple source domains without access to the target. A growing body of work disentangles domain-invariant degradation representations from domain-specific operational characteristics; for example, through split invariant/domain-dependent feature flows (Shao et al., 2025), joint autoencoders with shared and private extractors (Hu et al., 2022), mask-based disentanglement with information-theoretic constraints (Shang et al., 2024), and adversarial learning of conditional invariant and specific features (Xia et al., 2024). Such designs recognize that domain-specific features may correlate strongly with labels within individual domains and can therefore enhance performance on unseen data (Bui et al., 2021).

The research gap, therefore, lies in combining physics-based mechanistic insight with robust generalization under operating-condition shifts. The central question is how to design a prognostic model that (i) generalizes to unseen operating conditions and (ii) preserves physically consistent degradation dynamics. The present work addresses this question through a physics-informed domain generalization framework. Domain-invariant degradation features are separated from domain-specific operational characteristics, enabling zero-shot generalization to unseen load-speed regimes: marginal shifts are absorbed by the invariant representation, while conditional shifts are handled by intra-/extrapolating in the domain-specific representation. In parallel, fatigue-consistent behavior inspired by Paris-law dynamics is embedded as a soft structural prior in the architecture and loss function, constraining long-term RUL evolution to physically plausible, monotonic trajectories without enforcing fixed crack-growth paths.

The main contributions of this work are threefold:

1. A physics-informed domain generalization framework that disentangles domain-invariant degradation features from domain-specific operational characteristics, enabling zero-shot RUL prediction under unseen load-speed operating conditions.
2. A Paris-law-inspired physics regularization, introduced as a learning bias through a fatigue-consistency loss and Kullback-Leibler-regularized priors on the crack-growth parameters, which enforces physically plausible and monotonic degradation without imposing a rigid state-transition model and without increasing inference complexity.
3. Validation in a real-to-real transfer setting on experimental run-to-failure data, demonstrating improved prediction accuracy and monotonicity relative to a vanilla baseline and a standard domain generalization architecture.

The remainder of this paper is organized as follows. Section 2 reviews the theoretical background on fatigue crack growth, Paris' law, and Hertzian contact stress in rolling bearings. Section 3 presents the proposed physics-informed domain generalization methodology, including the physics-based loss function and the disentangled architecture. Section 4 describes the experimental case study and dataset, Section 5 reports and discusses the results, and Section 6 concludes the paper and outlines directions for future work.

2. THEORETICAL BACKGROUNDS

2.1. Fatigue Crack Growth and Paris' Law

Fatigue crack propagation in metallic components subjected to cyclic loading is commonly described within the

framework of LEFM. In this framework, the stress field near the crack tip is characterized by stress intensity factors (SIFs), which describe the amplitude of the singular stress field driving crack growth. Three fundamental fracture modes are typically defined: Mode I (opening mode), Mode II (in-plane shear or sliding mode), and Mode III (out-of-plane tearing mode). Mode I corresponds to tensile loading that opens the crack faces perpendicular to the crack plane, while Modes II and III represent shear displacements along and across the crack front, respectively (Hannes, 2014).

Under cyclic loading, the crack growth rate is commonly related to the stress intensity factor range

$$\Delta K = K_{max} - K_{min} \tag{1}$$

which represents the variation of the crack-tip driving force during a loading cycle. In the stable crack propagation regime, the relationship between crack growth rate and stress intensity factor range is commonly expressed by the Paris–Erdogan law:

$$\frac{da}{dN} = C(\Delta K)^m \tag{2}$$

where a is the crack length, N is the number of load cycles, and C and m are material-dependent parameters determined experimentally. Paris-law relationships describe crack growth primarily in the stable propagation regime (Stage II), after crack initiation (Kunzelmann et al., 2023)

In rolling contact fatigue, cracks are typically subjected to mixed-mode loading due to the combined action of Hertzian contact pressure and tangential traction generated by rolling-sliding contact. Numerical and experimental analyses of surface-initiated RCF cracks have demonstrated that the stress intensity factors evolve during over-rolling and that crack propagation often occurs under a combination of Mode I and Mode II loading, with Mode II shear frequently dominating the propagation behavior for longer cracks (Kunzelmann et al., 2023). To account for mixed-mode conditions, one commonly used equivalent stress intensity factor range is expressed as (Hannes & Alfredsson, 2012; Wong et al., 2000):

$$\Delta K_{eff} = \sqrt{\Delta K_I^2 + \Delta K_{II}^2} \tag{3}$$

which combines the opening and shear contributions into a single driving parameter for crack growth.

For rolling contact fatigue problems, the stress intensity factor in stage II of propagation is often expressed in terms of the maximum Hertzian contact pressure p_0, since the relevant stress components near the contact can be scaled with this characteristic stress level (Rycerz et al., 2017). As a result, in simplified RCF models, the stress intensity factor range can be approximated by the scaling relation $\Delta K_{eff} \propto p_0\sqrt{a}$ to characterize the driving force for crack propagation under rolling contact conditions (Rycerz et al., 2017). Such scaling relations provide a convenient link between contact mechanics and crack growth modeling, enabling Paris-law-based predictions of fatigue crack propagation and remaining useful life in rolling elements and bearing steels (Hannes & Alfredsson, 2012; Kunzelmann et al., 2023).

Together, these fracture mechanics formulations form the basis for many physics-based prognostic models, where Paris-law crack growth equations are embedded within state-space or hybrid physics-informed frameworks to estimate damage evolution and remaining useful life of mechanical components operating under cyclic loading.

2.2. Hertzian Contact Stress in Rolling Bearings

Rolling element bearings transmit loads through discrete contacts between the rolling elements and the raceway surfaces of the inner and outer rings. Due to the curved geometries involved, these contacts occur over very small areas, leading to highly concentrated stresses that must be evaluated using Hertzian contact theory. The geometry of the bearing, including the radii of curvature of the rolling elements and raceways, together with the applied external loads, determines the stress state within the contact region. Consequently, evaluation of the contact stresses requires first determining how the external load is distributed among the rolling elements.

Under radial loading conditions, the load carried by the bearing is not shared uniformly among all rolling elements. Instead, only the elements located within the load zone support significant loads, while elements outside this region carry little or no load. The load carried by an individual rolling element depends on its angular position relative to the direction of the applied load and on the elastic deformation of the contacting surfaces. The load on the *i*-th rolling element can be approximated by (Nguyen-Schäfer, 2016)

$$Q_i = Q_{max}\, Cos^n(\psi_i) \tag{4}$$

where Q_{max} denotes the maximum load carried by the most heavily loaded rolling element, ψ_i is the angular position of the element relative to the load direction, and n is an exponent related to the elastic contact behavior of the bearing system.

The element experiencing Q_{max} therefore governs the stress conditions within the bearing and is typically used for contact stress evaluation. Once the maximum rolling element load has been identified, the local contact stresses between the rolling element and the raceway can be evaluated using Hertzian theory. For ball bearings, the contact between the spherical rolling element and the raceway results in an elliptical contact area. The maximum

Hertzian contact pressure occurring at the center of this contact is given by (Nguyen-Schäfer, 2016)

$$p_0 = \frac{3Q_{max}}{2\pi ab} \tag{5}$$

where Q_{max} represents the maximum normal contact load and a and b are the semi-axes of the elliptical contact area. These dimensions depend on the elastic properties of the materials and the local curvature of the contacting bodies. The maximum contact pressure p_0 therefore provides a characteristic measure of the stress field generated within the rolling contact.

In practice, bearing analysis often focuses on the maximum contact stress at the most heavily loaded rolling element, as this location governs fatigue initiation and crack propagation processes in rolling contact fatigue. Detailed derivations of load distribution and Hertzian contact stress formulations can be found in classical bearing mechanics literature and comprehensive analyses of rolling bearing performance (Harris, 2001; Nguyen-Schäfer, 2016).

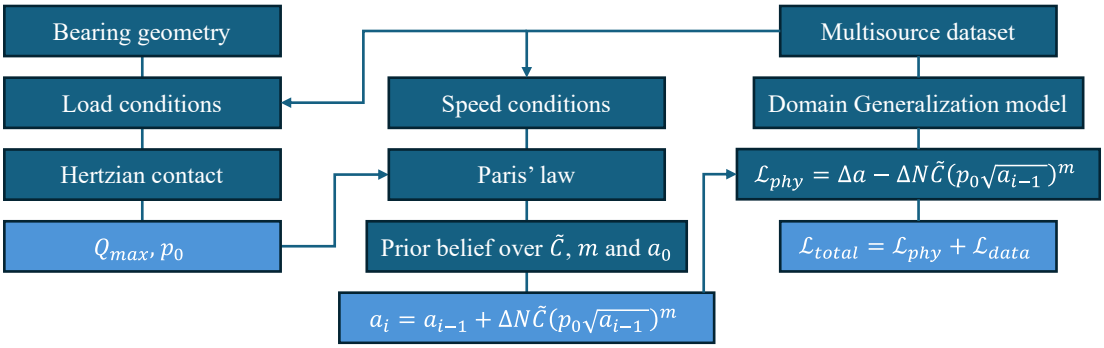

Figure 1. Workflow of the proposed method

3. PROPOSED METHODOLOGY

The proposed methodology integrates physics-based constraints with data-driven learning in order to regularize the remaining useful life prediction of rolling element bearings using the crack growth principles. Physics-informed machine learning approaches generally incorporate prior physical knowledge into learning algorithms through three primary mechanisms: I. Learning bias, II. Inductive bias, and III. Observational bias (Karniadakis et al., 2021). This study focuses primarily on the first approach, where the learning process is guided by additional loss terms derived from physical laws, forcing the model predictions to remain consistent with known physics during optimization. Specifically, the neural network predicts the parameters controlling fatigue crack growth, which are then used within the Paris' law formulation to constrain the learning process. This combination enables the model to maintain physical consistency while still adapting to variations observed in experimental data.

The overall workflow of the proposed approach is illustrated in Figure 1. First, the bearing geometry is used to calculate the required parameters for the calculation of Hertzian stress p_0. Second, Paris' law is formulated as a loss function that should be minimized during the training. This requires the model to output the crack length a_{i-1}, a_i and the parameters governing crack growth dynamics as the auxiliary outputs, which makes the latent space align with the physical constraints. Subsequently, the shared latent space is used to predict the remaining useful life of the bearing, and both the data-driven and physics-based errors are jointly minimized during training. This hybrid optimization framework allows the model to leverage both measurement information and prior physical knowledge to improve performance.

3.1. Physics-based Loss Function

For rolling contact fatigue in bearings, the stress field driving crack growth is strongly influenced by the local Hertzian contact stresses. Following previous studies, the stress intensity factor range can be approximated using the maximum Hertzian pressure p_0 and crack length a as $\Delta K_{eff} \propto p_0\sqrt{a}$. This approximation reflects the fact that the Hertzian contact pressure governs the stress distribution near the contact region, and therefore serves as a representative scaling parameter for the stresses acting on the crack tip. Using this formulation allows the effective stress intensity factor to capture the dominant loading conditions in rolling contact fatigue while avoiding the need to explicitly model the full stress field.

To account for uncertainties in loading conditions, material properties, and other unmodeled effects, the Paris' law coefficient C is replaced with an effective parameter $\tilde{C}$. This parameter implicitly absorbs the influence of unknown scaling factors and modeling simplifications. Therefore, a learning bias is introduced through the formulation of the following loss function. For this, the model outputs the unknown parameters $\tilde{C}$ and m as well as the crack length

a_{i-1} and a_i for two consecutive time instances. The $\mathcal{L}_{phy}$ is then defined as:

$$\mathcal{L}_{phy} = \frac{1}{M}\sum_{i=1}^{M}\left(a_i - a_{i-1} - \Delta N\tilde{C}\left(p_0\sqrt{a_{i-1}}\right)^m\right)^2 \quad (6)$$

where M is the number of available signals in the dataset.

Prior knowledge about typical crack growth parameters is incorporated through probabilistic priors on $\tilde{C}$ and m. These priors represent initial beliefs about physically plausible values derived from fatigue literature. During training, the neural network predicts parameter samples $\{\tilde{C}_i\}_{i=1}^{B}$ and $\{m_i\}_{i=1}^{B}$ for a mini-batch of size B, and $\{a_{0,q}\}_{q=1}^{Q}$ as the initial crack length values for the Q bearings in the training dataset. Instead of explicitly learning distribution parameters, stochastic estimators are obtained from empirical statistics. For $\tilde{C}$ and m, the empirical mean and variance are computed over the mini-batch, while for a_0, they are computed over the bearing-wise initial values

$$\hat{\mu}_\theta = \frac{1}{B}\sum_{i=1}^{B}\theta_i, \qquad \hat{\sigma}_\theta^2 = \frac{1}{B}\sum_{i=1}^{B}(\theta_i - \hat{\mu}_\theta)^2 \quad (7)$$

$$\hat{\mu}_{a_0} = \frac{1}{Q}\sum_{q=1}^{Q}a_{0,q}, \qquad \hat{\sigma}_{a_0}^2 = \frac{1}{Q}\sum_{q=1}^{Q}\left(a_{0,q} - \hat{\mu}_{a_0}\right)^2 \quad (8)$$

where $\theta \in \{\tilde{C}, m\}$. These statistics define an approximate Gaussian distribution $q(\theta) = \mathcal{N}(\hat{\mu}_\theta, \hat{\sigma}_\theta^2)$, which represents the current stochastic estimate of the parameter distribution during training. Similarly, the initial crack lengths $\{a_{0,q}\}_{q=1}^{Q}$ define an approximate Gaussian distribution $q(a_0) = \mathcal{N}(\hat{\mu}_{a_0}, \hat{\sigma}_{a_0}^2)$ based on their empirical statistics across the bearings. To constrain the learned parameters to remain consistent with prior physical knowledge, these distributions are regularized toward their respective prior distributions $p(\cdot) = \mathcal{N}(\mu_0, \sigma_0^2)$ for the parameters $\tilde{C}$, m and a_0 using the Kullback–Leibler (KL) divergence:

$$D_{KL}\big(q(\theta) \parallel p(\theta)\big) = log\frac{\sigma_0}{\hat{\sigma}_\theta} + \frac{\hat{\sigma}_\theta^2 + (\hat{\mu}_\theta - \mu_0)^2}{2\sigma_0^2} - \frac{1}{2} \quad (9)$$

The KL terms for three parameters are incorporated into the optimization objective as an additional regularization loss $\mathcal{L}_{KL}$. Since these parameters are treated as model outputs, they are allowed to deviate from the prior distributions when supported by the data.

3.2. Domain Generalization

The proposed framework is trained in a multi-source learning setting, where each source dataset corresponds to a different operating condition (e.g., different speeds, loads). The objective of the architecture is to learn representations that both preserve domain-dependent operational characteristics and extract degradation-related features that remain invariant across operating conditions.

The model receives as input the logarithmic power spectral density (log-PSD) of vibration signals measured from the bearing. For a vibration signal $x(t)$, the power spectral density is obtained as

$$S_{xx}(f) = \frac{1}{T}|X(f)|^2 \quad (10)$$

where $X(f)$ denotes the Fourier transform over a window of length T. The network input is defined as

$$\boldsymbol{x} = log\big(S_{xx}(f)\big) \quad (11)$$

Frequency-domain representations are particularly effective for bearing fault prognostics because localized defects generate spectral components at characteristic fault frequencies and their harmonics.

Before entering the model, the inputs are normalized using the empirical mean and standard deviation of the training set

$$\tilde{x} = \frac{x - \mu_{train}}{\sigma_{train}} \quad (12)$$

As illustrated in Figure 2, the architecture processes two consecutive temporal inputs, $\tilde{\boldsymbol{x}}_{i-1}$ and $\tilde{\boldsymbol{x}}_i$. Using two time instances allows the model to capture the temporal evolution of degradation and estimate both the previous and current crack states, which is consistent with fatigue crack growth processes that evolve incrementally over time.

Two parallel feature extractors are employed to disentangle the latent representation into domain-specific and domain-invariant components. The extractor $F_S(\cdot)$ learns domain-specific representations

$$z_{S_i} = F_S(\tilde{\boldsymbol{x}}_i) \quad (13)$$

while the second extractor $F_I(\cdot)$ learns domain-invariant representations

$$z_{I_i} = F_I(\tilde{\boldsymbol{x}}_i) \quad (14)$$

To guide the extractors toward learning these representations, two domain classifiers G_S and G_I are introduced. The classifier G_S operates on the domain-specific features and predicts the operating condition label

$$o_{S_i} = G_S\big(z_{S_i}\big) \quad (15)$$

The corresponding loss function is defined using the cross-entropy criterion

$$\mathcal{L}_S = -\frac{1}{M}\sum_{i=1}^{M}\sum_{k=1}^{K} c_i^{(k)}\, log\, o_{S_i}^{(k)} \tag{16}$$

where $o_{S_i}^{(k)}$ denotes the k-th output of the classifier. K is the number of source domains, and $c^{(k)}$ is domain label, where $c^{(k)} = 1$ for the correct operating condition and 0 for the remaining domains. This loss encourages F_S to preserve information that helps discriminate between operating conditions.

The second classifier G_I is connected to the invariant features through a gradient reversal layer (GRL). During forward propagation, the GRL acts as an identity mapping, but during backpropagation, it reverses the gradient.

$$R_\lambda(x) = x$$
$$\frac{dR_\lambda}{dx} = -\lambda I \tag{17}$$

where I is the identity matrix and λ controls the adversarial strength. The classifier, therefore, receives

$$o_{I_i} = G_I\left(R_\lambda(z_{I_i})\right) \tag{18}$$

The cross-entropy loss associated with this classifier is

$$\mathcal{L}_I = -\frac{1}{M}\sum_{i=1}^{M}\sum_{k=1}^{K} c_i^{(k)}\, log\, o_{I_i}^{(k)} \tag{19}$$

During training, the classifier G_I attempts to maximize its domain classification accuracy, while the gradient reversal forces the feature extractor F_I to minimize this accuracy. This adversarial interaction prevents the classifier from distinguishing between domains, meaning that the features extracted by F_I become domain-invariant.

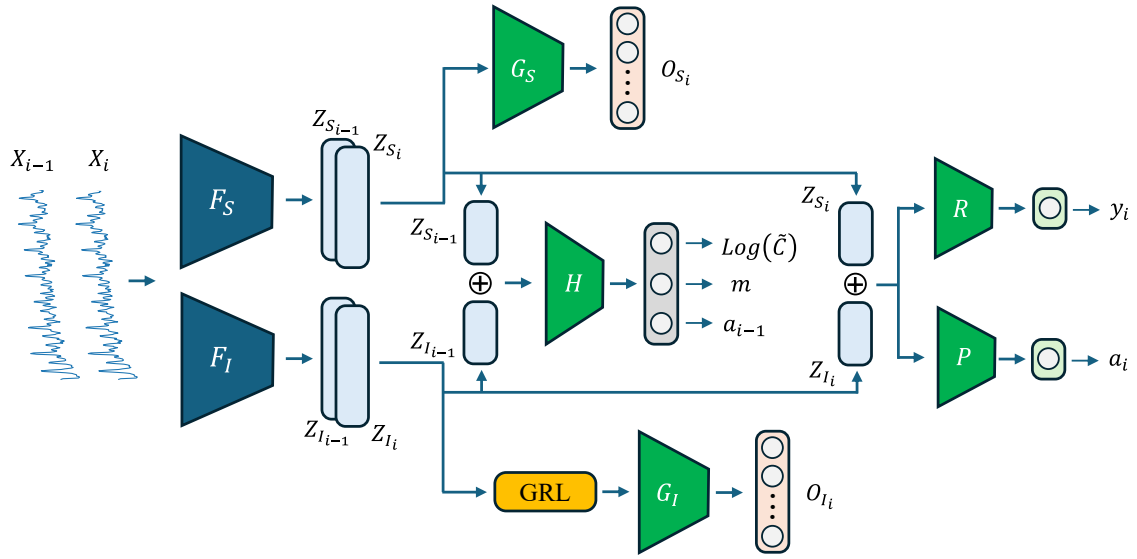

Figure 2. Proposed model architecture

The disentanglement condition between two groups of features, Z_{I_i} and Z_{S_i}, can be solved by forcing their covariance matrix close to zero (Bui et al., 2021). Loss function $\mathcal{L}_{cov}$ is defined as follows:

$$\mathcal{L}_{cov} = \frac{1}{M}\sum_{i=1}^{M}\left(Cov\left(Z_{I_i}, Z_{S_i}\right)\right)^2 \tag{20}$$

To incorporate fatigue crack propagation physics, the model includes a module H that receives the latent features from the previous time step are fused ($Z_{S_{i-1}} \oplus Z_{I_{i-1}}$) and estimates the parameters governing crack growth. The outputs of this module are $Log(\tilde{C})$, m and a_{i-1}. Finally, the latent representations of the current input are fused ($Z_{S_i} \oplus Z_{I_i}$) and passed to the prediction heads. The regressor R estimates the remaining useful life $y_i = R\left(Z_{S_i} \oplus Z_{I_i}\right)$, and module P estimates the crack state $a_i = P\left(Z_{S_i} \oplus Z_{I_i}\right)$. The RUL prediction is trained using the mean squared error (MSE) loss

$$\mathcal{L}_{RUL} = \frac{1}{M}\sum_{i=1}^{M}(\hat{y}_i - y_i)^2 \tag{21}$$

where y_i and $\hat{y}_i$ denote the true and predicted RUL values for the i-th signal in the dataset, respectively.

Finally, the total loss function that should be minimized during training is

$$\mathcal{L}_{total} = \mathcal{L}_{phy} + \mathcal{L}_{KL} + \mathcal{L}_S + \mathcal{L}_I + \mathcal{L}_{cov} + \mathcal{L}_{RUL} \quad (22)$$

Through the combination of multi-source adversarial training, disentangled representation learning, and physics-informed degradation modeling, the proposed architecture simultaneously captures operational variability and invariant degradation behavior, enabling robust prognostic performance across unseen operating conditions.

4. CASE STUDY

The publicly available XJTU run-to-failure dataset is well-suited to this study, as its multiple operating conditions provide the distinct source and target domains required to evaluate generalization under realistic domain discrepancies commonly encountered in industrial applications. The test setup contains an AC motor, a speed controller, a support shaft with two mounted bearings, and a hydraulic loading module applying radial load to the tested bearing (B. Wang et al., 2020). The tested rolling element bearing is of LDK UER204 type, and fifteen full degradation tests have been realized, five for each operating condition, as shown in Table 1. Vibration signals are collected with a sampling frequency of 25.6 kHz by two accelerometers mounted in the horizontal and vertical directions on the housing of the tested bearing. The observed faults at the end of the tests are listed in Table 1. The sampling duration of each signal is 1.28 s (32,768 points), and the signal collection interval is 1 minute during the whole measurement campaign. Figure 3 shows the image of the test setup with its components.

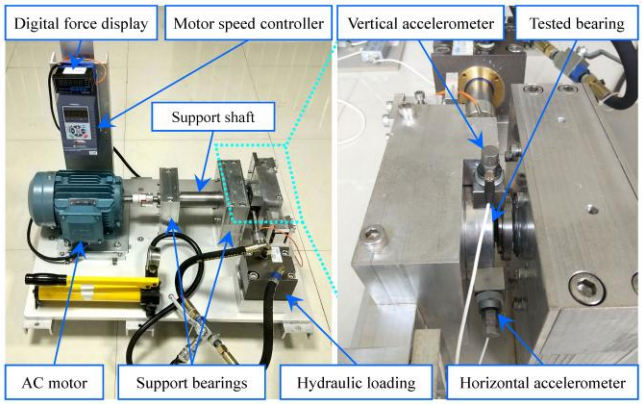

Figure 3. XJTU bearing test setup (B. Wang et al., 2020)

Table 1. XJTU dataset information

Operating condition	Bearing	Test duration	Fault
2100 rpm/12 kN	1-1	123 min.	OR
	1-2	161 min.	OR
	1-3	158 min.	OR
	1-4	122 min.	Cage
	1-5	52 min.	IR & OR
2250 rpm/11 kN	2-1	491 min.	IR
	2-2	161 min.	OR
	2-3	533 min.	Cage
	2-4	42 min.	OR
	2-5	339 min.	OR
2400 rpm/10 kN	3-1	2538 min.	OR
	3-2	2496 min.	IR & Ball & Cage & OR
	3-3	371 min.	IR
	3-4	1515 min.	IR
	3-5	114 min.	OR

5. RESULTS AND DISCUSSIONS

Three scenarios for domain generalization and multisource training are considered based on the XJTU dataset: training with the run-to-failure datasets from two operating conditions and testing on another one. To begin with, the prior beliefs for the three parameters introduced in Section 3.1 are specified in Table 2, selected to be close to values reported in the literature (Bhadeshia, 2012; Kunzelmann et al., 2023).

Table 2. Prior distributions of parameters, $\tilde{C}$, m and a_0

Parameter	$log_{10}\,\tilde{C}$	m	a_0
Prior distribution	$\mathcal{N}(-12, 1)$	$\mathcal{N}(3, 0.25)$	$\mathcal{N}(0.1, 0.01)$

Table 3 presents the calculation results obtained from the Hertzian contact formulations described in (Harris, 2001; Nguyen-Schäfer, 2016). The detailed calculations are mentioned in the Appendix. The parameter p_0 reported in Table 3 represents the maximum Hertzian contact stress between the ball in the middle of the load zone and the outer race, which is the highest Hertzian stress in the bearing according to the calculations in the Appendix. The quantity ΔN is computed from the rotational speed and the time

interval between the measurements, which is 1 minute in the XJTU dataset, and expressed in million cycles, while the crack length a is in millimeters. Although the stress cycles experienced by individual bearing components do not exactly correspond to the shaft rotation cycles, they can be scaled proportionally from the rotational speed. Furthermore, the stress magnitude at a given point on the inner race or rolling elements varies as these components pass through the load zone and experience different load levels. These sources of uncertainty and modeling simplifications are effectively absorbed by the parameter $\tilde{C}$ during training.

In this study, prognostics begins at the First Prediction Time (FPT), defined as the first point where the peak-to-peak amplitude of the vibration signal exceeds a threshold computed from the healthy baseline as the mean plus three standard deviations. This indicates the onset of detectable degradation, after which the prognostic model starts estimating the remaining useful life. The end of life (EOL) is defined at a peak-to-peak level of 50 g, as most bearings in the dataset operate up to approximately this value. Any data beyond this level is truncated to ensure a consistent definition of EOL across all bearings.

Table 3. Calculated Hertzian contact stress and stress cycles

Parameter/ Operating conditions	p_0 (GPa)	Q_{max} (kN)	ΔN (million cycles)
2100 rpm/ 12 kN	4.21	6.57	2100×10^{-6}
2250 rpm/ 11 kN	4.09	6.03	2250×10^{-6}
2400 rpm/ 10 kN	3.96	5.48	2400×10^{-6}

Table 4 details the proposed model architecture illustrated in Figure 2.

Table 5 presents the results of three models for comparison:

- Vanilla model: the basic model, which only consists of feature extractors F_S and F_I. Domain classifiers are ineffective, and the model is not physics-informed.
- DG model: it consists of feature extractors and two domain classifiers. The model is not physics-informed.
- Physics-informed model: the proposed physics-informed domain generalization model.

It should be noted that the complexity of the feature extractors F_S and F_I and regressor R are the same in all models, which means that in the inference stage, all the models have the same complexity, because the other parts of the proposed model are just regularizers in training.

Table 4. Details of the proposed model

Feature Extractor F_S		**Feature Extractor F_I**	
Layer	**CH/K/S/P***	**Layer**	**CH/K/S/P**
CNN 1	8/16/2/2	CNN 4	8/16/2/2
CNN 2	16/8/2/2	CNN 5	16/8/2/2
CNN 3	16/4/2/2	CNN 6	16/4/2/2
Flatten	-	Flatten	-

Classifier G_S		**Classifier G_I**	
Layer	**Unit**	**Layer**	**Unit**
Dense 1	K/Softmax	Dense 2	K/ Softmax

Predictor H		**Regressor P**		**Regressor R**	
Layer	**Unit**	**Layer**	**Unit**	**Layer**	**Unit**
Dense 3	12	Dense 5	12	Dense 7	12
Dense 4	3	Dense 6	1	Dense 8	1

*CH: channels, K: kernel, S: stride, P: max pooling

To compare the performance of the prognostic models, two metrics are used: Root Mean Square Error (RMSE) and monotonicity (MN):

$$RMSE = \sqrt{\frac{1}{M}\sum_{i=1}^{M}(\hat{y}_i - y_i)^2} \tag{23}$$

$$MN = 100 \times \left| \frac{1}{M-1} \sum_{i=1}^{M-1} sign(\hat{y}_{i+1} - \hat{y}_i) \right| \ (\%) \tag{24}$$

Figure 4 shows the predicted RUL for bearing 2-5 in training scenario 1,3 → 2. It shows how the domain generalization and the proposed physics-informed model enhance the predictive performance. Not only is the predicted RUL more accurate, but it is also more monotonic by incorporating the physics of failure into the model. The confidence intervals are estimated from an ensemble of trained models using the variance of their outputs for the same input.

Table 5 presents the results for three training scenarios, where data from one operating condition is held out for testing while the model is trained on the remaining conditions. The results indicate that the physics-informed model is able to enhance the performance in most of the cases, either interpolation or extrapolation in the operating-condition space. This suggests that the learning bias

introduced by Paris' law improves both extrapolation and interpolation capabilities in the operating-condition space. Moreover, the proposed model does not increase inference complexity since the physics-based modules act only as training regularizers.

The large prediction error for bearing 3-2 may be explained by the presence of multiple failure modes in the dataset, including inner race, outer race, ball, and cage faults. Since these mechanisms produce different degradation patterns, trained models may find it difficult to predict the RUL effectively.

Table 5. Implementation results for three models; RMSE is in terms of minutes, MN in percentage

Scenario	Bearing	Vanilla model		DG model		Physics-informed model	
		RMSE ↓	MN ↑	RMSE ↓	MN ↑	RMSE ↓	MN ↑
1, 3 → 2	2-1	**6.4**	2.9	10.1	2.9	9.5	**14.3**
	2-2	52.2	5.8	22.1	**16.3**	**19.7**	12.5
	2-3	23.9	6.9	15.0	15.5	**10.8**	**20.7**
	2-4	2.1	**75.0**	1.9	25.0	**1.8**	**75.0**
	2-5	42.8	3.8	28.6	8.9	**22.1**	**13.9**
2, 3 → 1	1-1	9.3	34.8	8.7	34.8	**7.1**	**56.5**
	1-2	35.5	5.9	**28.6**	10.9	33.0	**12.6**
	1-3	11.5	14.3	14.6	27.5	**8.0**	**40.7**
	1-4	15.8	2.6	14.9	**23.1**	**12.4**	7.7
	1-5	2.5	14.3	2.1	28.6	**1.7**	**57.1**
1, 2 → 3	3-1	20.4	14.5	13.4	24.2	**7.3**	**27.4**
	3-2	**150.0**	5.0	167.5	0.9	168.2	**5.5**
	3-3	2.5	**66.7**	**2.2**	50.5	**2.2**	50.0
	3-4	22.2	16.1	19.8	**18.3**	**13.3**	9.7
	3-5	21.1	23.9	18.1	9.9	**14.9**	**26.8**
Avg.	-	27.9	19.5	24.5	19.8	**22.1**	**28.7**

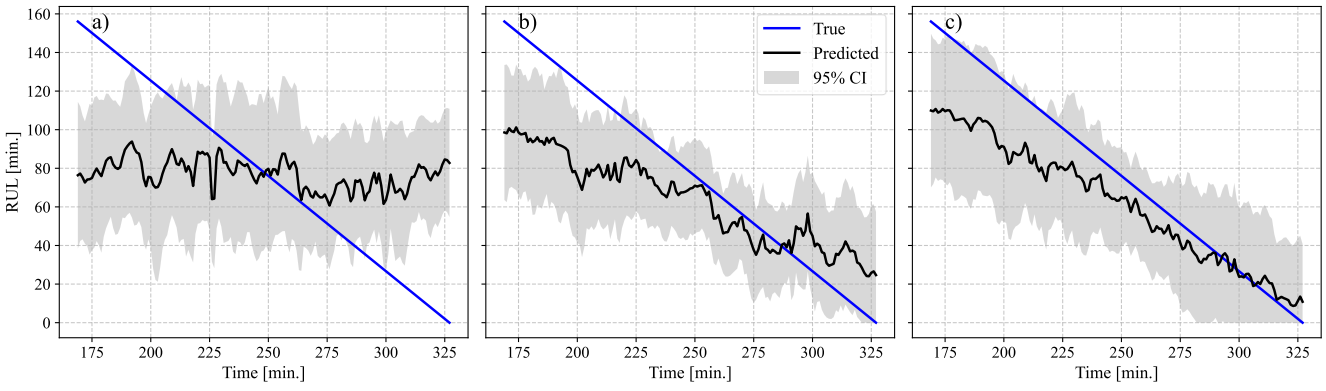

Figure 4. Predicted RUL for bearing 2-5 in scenario 1, 3 → 2; a) Vanilla model, b) DG model, c) Physics-informed model

Moreover, Figure 5 shows the estimated crack length for three bearings under three different scenarios of domain generalization. For bearing 2-5, where the task corresponds to interpolation between different load-speed operating conditions, the estimated crack growth follows the expected dynamics more closely and exhibits monotonic behavior. In contrast, for bearings 1-2 and 3-1, the proposed model shows difficulty maintaining a monotonic trajectory in the estimated crack growth. This behavior is consistent with a classical phenomenon in machine learning models, where interpolation within the training distribution is generally easier than extrapolation to unseen regions of the operating-

condition space. Nevertheless, Table 5 indicates that the physics-informed model still improves predictive performance in extrapolation scenarios compared to the baseline approaches.

It is worth noting that for the run-to-failure tests in which no crack length has been measured or observed, it is not possible to correctly estimate the true crack length with the proposed approach, as there are many uncertainties in play. Therefore, the aim of incorporating Paris' law is to construct a physics-consistent damage indicator that is closely linked to the damage severity. This can regularize the latent space or the deep features extracted by the model to be more aligned with the physics of failure, resulting in a higher performance.

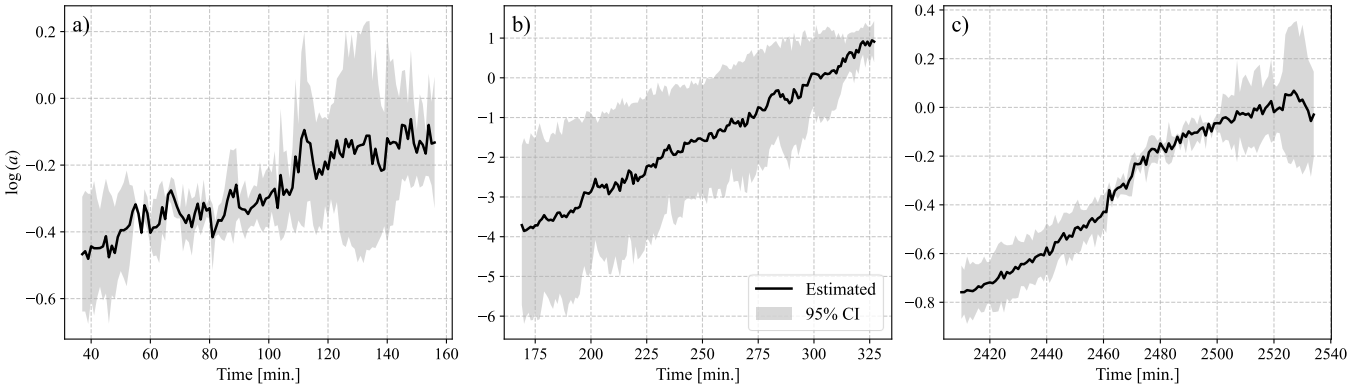

Figure 5. Estimated crack length (damage indicator) by the proposed model for bearing a) 1-2, b) 2-5, c) 3-1

6. CONCLUSION

This study presented a physics-informed domain generalization framework for remaining useful life prediction of rolling element bearings under unseen operating conditions. The proposed approach integrates feature disentanglement with physics-based regularization derived from Paris-law crack growth dynamics. By separating domain-invariant degradation features from domain-specific operational characteristics, the model enables zero-shot generalization across different load-speed regimes while maintaining physically consistent degradation trajectories.

The physics-informed loss introduces a learning bias that constrains the latent degradation representation to follow fatigue-consistent behavior without enforcing rigid physical models. Experimental evaluation on the XJTU run-to-failure dataset demonstrates that the proposed method improves prognostic robustness compared to conventional data-driven models and standard domain generalization architectures. In particular, the integration of physics-based regularization enhances the monotonicity and stability of the predicted RUL trajectories while maintaining competitive prediction accuracy.

Although the estimated crack length should be interpreted as a damage indicator rather than a direct physical measurement, the results show that embedding fatigue crack growth principles provides meaningful structural guidance for learning degradation patterns. Future work will focus on incorporating more detailed contact-mechanics modeling, extending the framework to additional operating regimes and datasets, and investigating probabilistic formulations that further quantify uncertainty in physics-informed prognostics.

ACKNOWLEDGEMENT

This research is (partly) funded by the Flanders AI Research Program, an initiative of the Flemish Government. The authors also gratefully acknowledge the support of Flanders Make, the strategic research center for the manufacturing industry, in the context of the Lobber project, as well as the Flemish Supercomputer Center (VSC) for providing the computational resources.

REFERENCES

Bhadeshia, H. K. D. H. (2012). Steels for bearings. *Progress in Materials Science*, *57*(2), 268–435. https://doi.org/10.1016/j.pmatsci.2011.06.002

Bui, M.-H., Tran, T., Tran, A. T., & Phung, D. (2021). Exploiting Domain-Specific Features to Enhance Domain Generalization. *Proceedings of the 35th International Conference on Neural Information Processing Systems, NIPS '21*, 21189–21201.

Chen, J., Yuan, S., Qiu, L., Wang, H., & Yang, W. (2018). On-line prognosis of fatigue crack propagation based on Gaussian weight-mixture proposal particle filter. *Ultrasonics*, *82*, 134–144. https://doi.org/10.1016/j.ultras.2017.07.016

Da Costa, P. R. D. O., Akçay, A., Zhang, Y., & Kaymak, U. (2020). Remaining useful lifetime prediction via deep domain adaptation. *Reliability Engineering &*

System Safety, *195*, 106682. https://doi.org/10.1016/j.ress.2019.106682

Dhibi, K., Nounou, H., El-Mellouhi, F., & Nounou, M. (2026). Physics-Informed Deep Learning for Bearing Remaining Useful Life: Adaptive Paris-Law Regularization with Gaussian Processes. *Integrating Materials and Manufacturing Innovation*. https://doi.org/10.1007/s40192-026-00441-w

Dong, S., Xiao, J., Hu, X., Fang, N., Liu, L., & Yao, J. (2023). Deep transfer learning based on Bi-LSTM and attention for remaining useful life prediction of rolling bearing. *Reliability Engineering & System Safety*, *230*, 108914. https://doi.org/10.1016/j.ress.2022.108914

Han, Y., Liu, K., Cui, T., Zhang, Y., Hu, A., & Huang, Q. (2026). Domain generalization for remaining useful life prediction of rolling bearings based on analogous synaptic consolidation under unseen conditions. *Measurement*, *258*, 119081. https://doi.org/10.1016/j.measurement.2025.119081

Hannes, D. (2014). *On fatigue crack growth modelling of surface initiated rolling contact fatigue using the asperity point load mechanism*. PhD dissertation, Engineering Sciences, KTH Royal Institute of Technology. https://urn.kb.se/resolve?urn=urn:nbn:se:kth:diva-141151

Hannes, D., & Alfredsson, B. (2012). A fracture mechanical life prediction method for rolling contact fatigue based on the asperity point load mechanism. *Engineering Fracture Mechanics*, *83*, 62–74. https://doi.org/10.1016/j.engfracmech.2011.12.012

Harris, T. A. (2001). *Rolling bearing analysis* (4. ed). Wiley.

Hosseinli, S. A., Ooijevaar, T., & Gryllias, K. (2023). Context-aware machine learning for estimating the remaining useful life of bearings under varying speed operating conditions. *Annual Conference of the PHM Society*, *15*(1). https://doi.org/10.36001/phmconf.2023.v15i1.3571

Hosseinpour, F., Behzad, M., & Zio, E. (2020). Model-based Prognostic of the Remaining Useful Life of Bearings Considering Model Parameter Uncertainty. *Proceedings of the 30th European Safety and Reliability Conference and 15th Probabilistic Safety Assessment and Management Conference*, 3650–3655. https://doi.org/10.3850/978-981-14-8593-0_5831-cd

Hu, T., Guo, Y., Gu, L., Zhou, Y., Zhang, Z., & Zhou, Z. (2022). Remaining useful life prediction of bearings under different working conditions using a deep feature disentanglement based transfer learning method. *Reliability Engineering & System Safety*, *219*, 108265. https://doi.org/10.1016/j.ress.2021.108265

Karniadakis, G. E., Kevrekidis, I. G., Lu, L., Perdikaris, P., Wang, S., & Yang, L. (2021). Physics-informed machine learning. *Nature Reviews Physics*, *3*(6), 422–440. https://doi.org/10.1038/s42254-021-00314-5

Kunzelmann, B., Rycerz, P., Xu, Y., Arakere, N. K., & Kadiric, A. (2023). Prediction of rolling contact fatigue crack propagation in bearing steels using experimental crack growth data and linear elastic fracture mechanics. *International Journal of Fatigue*, *168*, 107449. https://doi.org/10.1016/j.ijfatigue.2022.107449

Liu, X., Jia, Y., He, Z., & Sun, L. (2017). Hybrid residual fatigue life prediction approach for gear based on Paris law and particle filter with prior crack growth information. *Journal of Vibroengineering*, *19*(8), 5908–5919. https://doi.org/10.21595/jve.2017.18327

Nguyen-Schäfer, H. (2016). *Computational Design of Rolling Bearings*. Springer International Publishing. https://doi.org/10.1007/978-3-319-27131-6

Rycerz, P., Olver, A., & Kadiric, A. (2017). Propagation of surface initiated rolling contact fatigue cracks in bearing steel. *International Journal of Fatigue*, *97*, 29–38. https://doi.org/10.1016/j.ijfatigue.2016.12.004

Shang, J., Qiu, H., & Gao, L. (2024). A Mask Disentanglement Domain Generalization Method for Bearings Remaining Useful Life Prediction Under Unknown Operating Conditions. *2024 Global Reliability and Prognostics and Health Management Conference (PHM-Beijing)*, 1–6. https://doi.org/10.1109/PHM-Beijing63284.2024.10874586

Shao, Y., Wang, C., Jia, Q., & Zhao, W. (2025). Comprehensive disentanglement with fine-grained feature mitigation for domain generalization. *Neural Networks*, *191*, 107757. https://doi.org/10.1016/j.neunet.2025.107757

Shi, H., Yang, T., Song, Z., Bai, X., Li, T., Gao, T., & Ma, H. (2026). A hybrid digital twin model for quantitative prediction of defect sizes and acceleration responses of rolling bearings with sparse measured data. *Measurement*, *257*, 118753. https://doi.org/10.1016/j.measurement.2025.118753

Ta, Y., Wang, T., Xie, J., Pan, T., & Wang, Z. (2026). Physics-driven prediction method for remaining useful life of rolling bearings incorporating Paris' fatigue damage mechanism. *Engineering*

Applications of Artificial Intelligence, *170*, 114196. https://doi.org/10.1016/j.engappai.2026.114196

Wang, B., Lei, Y., Li, N., & Li, N. (2020). A Hybrid Prognostics Approach for Estimating Remaining Useful Life of Rolling Element Bearings. *IEEE Transactions on Reliability*, *69*(1), 401–412. https://doi.org/10.1109/TR.2018.2882682

Wang, L., Zhang, C., Tao, C., Ji, H., Yang, Y., & Qiu, J. (2023). Prediction of multiple fatigue crack growth based on modified Paris model with particle filtering framework. *Mechanical Systems and Signal Processing*, *190*, 110124. https://doi.org/10.1016/j.ymssp.2023.110124

Wong, S. L., Bold, P. E., Brown, M. W., & Allen, R. J. (2000). Fatigue crack growth rates under sequential mixed-mode I and II loading cycles. *Fatigue & Fracture of Engineering Materials & Structures*, *23*(8), 667–674. https://doi.org/10.1046/j.1460-2695.2000.00342.x

Xia, P., Huang, Y., Qin, C., & Liu, C. (2024). Towards prognostic generalization: A domain conditional invariance and specificity disentanglement network for remaining useful life prediction. *Journal of Intelligent Manufacturing*, *35*(7), 3459–3477. https://doi.org/10.1007/s10845-023-02215-z

Yucesan, Y. A., & Viana, F. A. C. (2023). A Physics-informed Neural Network for Wind Turbine Main Bearing Fatigue. *International Journal of Prognostics and Health Management*, *11*(1). https://doi.org/10.36001/ijphm.2020.v11i1.2594

BIOGRAPHIES

Seyed Ali Hosseinli received his BSc in Railway Engineering from the Iran University of Science and Technology (IUST) and his MSc in Mechanical Engineering from the Sharif University of Technology (SUT). He is currently a Ph.D. researcher in the Department of Mechanical Engineering at KU Leuven, Belgium. His research interests center on machine learning techniques for prognostics and fault diagnostics of rotary equipment.

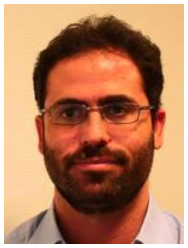

Konstantinos Gryllias holds a 5-year engineering diploma degree and a Ph.D. degree in Mechanical Engineering from the National Technical University of Athens, Greece. He holds a professor position on vibro-acoustics of machines and transportation systems at the Department of Mechanical Engineering of KU Leuven, Belgium. He is also the manager of the University Core Lab Flanders Make@KU Leuven - MPro of Flanders Make, Belgium. His research interests lie in the fields of condition monitoring, signal processing, prognostics, and health management of mech. & mechatronic systems.

Appendix

The following calculations are followed to realize the maximum Hertzian stresses between the bearing components used in the XJTU dataset. Table A.1 details the LDK UER204 bearing specifications in the XJTU dataset mentioned by (Shi et al., 2026).

Table A.1. LDK UER204 bearing specifications

Parameter	Value	Parameter	Value
Pitch diameter (mm)	34.55	Number of balls	8
Ball diameter (mm)	7.92	Clearance (mm)	0.003
Contact angle (°)	0.00		

The following formulas are adopted from the work of (Harris, 2001; Nguyen-Schäfer, 2016). To begin with, the curvature differences of inner and outer races ($F_{b/IR}$ and $F_{b/OR}$) for ball bearings are calculated using

$$F_{b/IR} = \frac{A + 2\kappa_i - 1}{A(4\kappa_i - 1) - 2\kappa_i + 1} \tag{A.1}$$

$$F_{b/OR} = \frac{A - 2\kappa_o - 1}{A(4\kappa_o - 1) + 2\kappa_o + 1} \tag{A.2}$$

$$A = \frac{D_p}{D_b \cos(\alpha)} \tag{A.3}$$

where κ_i and κ_o are bearing inner and outer osculations, respectively. D_p and D_b are the pitch and ball diameters in bearing, respectively, and α is the contact angle. A is calculated as 4.63. According to the standard common values for $\kappa_i = 0.51$ and $\kappa_o = 0.53$, the curvature differences $F_{b/IR}$ and $F_{b/OR}$ are calculated as 0.97 and 0.87, respectively. By having the curvature differences and using Table 6.1 by (Harris, 2001), the dimensionless contact deformations δ^*_{IR} and δ^*_{OR} are found to be 0.51 and 0.72, respectively. Load-deflection factor K is then defined as:

$$K = 2.15 \times 10^5 \left(\sum \rho_b\right)^{-0.5} (\delta^*)^{-1.5} \tag{A.4}$$

$$\sum \rho_{b/IR} = \frac{2}{D_b}\left(2 + \frac{1}{A-1} - \frac{1}{2\kappa_i}\right) \tag{A.5}$$

$$\sum \rho_{b/OR} = \frac{2}{D_b}\left(2 - \frac{1}{A+1} - \frac{1}{2\kappa_o}\right) \tag{A.6}$$

where $\sum \rho_{b/IR}$ and $\sum \rho_{b/OR}$ are the curvature sum of the rolling element and inner race or outer race and obtained as

0.33 and 0.22, respectively. Therefore, parameters K_{IR} and K_{OR} are calculated as 1035187.7 and 749018.1. The overall load-deflection factor K_n is then calculated as:

$$K_n = \left(\frac{1}{(1/K_{IR})^{1/1.5} + (1/K_{OR})^{1/1.5}}\right)^{1.5} \quad \text{(A.7)}$$

which results in K_n to be 310740.2. Finally, to find the maximum load carried by the ball in the load zone, Q_{max}, the following equations should be numerically solved:

$$F_r = ZK_n\left(\delta_r - \frac{e}{2}\right)^{1.5} J_r(\epsilon) \quad \text{(A.8)}$$

$$\epsilon = 0.5\left(1 - \frac{e}{2\delta_r}\right) \quad \text{(A.9)}$$

where Z is the number of the balls, and e is the radial clearance. δ_r is the ring radial shift occurring at the middle of the load zone. For a given bearing under radial load F_r, an initial value of ϵ is assumed, from which the corresponding radial deflection δ_r is computed using the geometric relation between clearance and deformation in Equation A.9. The function $J_r(\epsilon)$ is then obtained from tabulated values in Table 7.1 by (Harris, 2001) via interpolation. This value is substituted into Equation A.8, and the process is repeated until convergence is achieved, yielding consistent values of ϵ, $J_r(\epsilon)$ and δ_r. The calculation results are therefore: $\epsilon = 0.49675$, $J_r(\epsilon) = 0.22824$, and $\delta_r = 0.07698$.

Finally, Equation A.10 is used to find the Q_{max}:

$$F_r = ZQ_{max}J_r(\epsilon) \quad \text{(A.10)}$$

which results in 6571.9 *N*, 6025.1 *N*, and 5478.3 *N* for the three radial load cases mentioned in the XJTU dataset as 12 *kN*, 11 *kN*, and 10 *kN*, respectively.

The maximum Hertzian stress p_0 is calculated using the following equations:

$$p_0 = \frac{3Q_{max}}{2\pi ab} \quad \text{(A.11)}$$

$$a = \xi \cdot \left(\frac{3Q_{max}}{E' \sum \rho_b}\right)^{1/3} \quad \text{(A.12)}$$

$$b = \eta \cdot \left(\frac{3Q_{max}}{E' \sum \rho_b}\right)^{1/3} \quad \text{(A.13)}$$

$$E' = \frac{2}{\left(\frac{1-\vartheta_1^2}{E_1} + \frac{1-\vartheta_2^2}{E_2}\right)} \quad \text{(A.14)}$$

where a and b are the semimajor and semiminor axes of the elliptic contact zone, and ξ and η are the dimensionless semiminor and semimajor axes. E and ϑ are the modulus of elasticity and Poisson's ratio, respectively. E' is the effective modulus of elasticity of the ball and raceways. Following the procedure outlined in Section 3.2 by (Nguyen-Schäfer, 2016), the parameters a and b are obtained as mentioned in Table A.2 for the contact between the ball in the middle of the load zone and the inner race or outer race.

Table A.2. Axes of the elliptic contact zone in mm

Parameter / Load case	a_{OR}	b_{OR}	a_{IR}	b_{IR}
12 kN	2.05	0.36	3.28	0.23
11 kN	2.00	0.35	3.18	0.22
10 kN	1.93	0.34	3.09	0.22

which results in maximum Hertzian stress p_0 between the ball in the middle of the load zone and outer race or inner race as mentioned in Table A.3.

Table A.3. Maximum Hertzian stress in GPa

Parameter / Load case	$p_{0,IR}$	$p_{0,OR}$
12 kN	4.16	4.21
11 kN	4.05	4.09
10 kN	3.92	3.96